TerraLock: A Dynamic Trekking Pole Design for Outdoor Accessibility

Ben Chern, Liam Cootey, Berzelai Ponce Lopez, Noah Thomas, Max Zeng

The authors are with the Department of Mechanical Engineering, Columbia University, New York, NY blc2145@columbia.edu, lsc2185@columbia.edu, bep2127@columbia.ed, nst2121@columbia.edu, zz3182@columbia.edu. This material is based upon work developed in the MECE E3420 / E3430 Engineering Design Courses

Abstract— **This paper presents the design, fabrication, and testing of a granular jamming trekking pole intended to improve stability and accessibility for hikers. A vacuum-driven pump, triggered by limit switches and controlled via an Arduino microcontroller, evacuates air from a coffee-ground-filled membrane to stiffen the pole on demand when contact with the ground is detected. Mechanical testing confirmed that the membrane withstood puncture from sharp implements, a compressive load of 54 lb (240 N), and a drop test, while the 3D printed coupler sustained a shear load of 50 lb (222 N) without failure. Electrically, the pump drew considerably less current than estimated in practice, yielding a projected battery life of 6–12 hours on a 6000 mA-h battery. The final prototype successfully demonstrated granular jamming under real operating conditions. While testing was primarily qualitative, the results are encouraging and suggest the design is a viable proof of concept for a adaptive assistive hiking device. Future work should focus on instrumented mechanical validation, coupler optimization, and field testing under real hiking conditions.**

I. Introduction

Trekking poles are a critical piece of hiking equipment, yet conventional designs offer limited adaptability across varying terrain, posing safety risks for users with limited mobility [1]. This project addresses that gap through a granular jamming trekking pole (Fig. 1) that transitions between soft and rigid states on demand [2]. When the user loads the pole, a pressure sensor triggers a vacuum pump that evacuates air from a coffee-ground-filled membrane, stiffening the structure. Releasing the pole from the surface returns the membrane to a flexible state. The key idea behind this product's design was the use of granular jamming to create a membrane that could conform to any surface on which it was placed, thereby providing stability to the user. Refer to Fig. 2 to observe the unjammed and jammed states of the membrane. The five main design constraints were: determining an appropriate holding force, performing electrical analysis, applying FEA to the prospective pole coupler, conducting membrane puncture tests, and performing shear load testing.

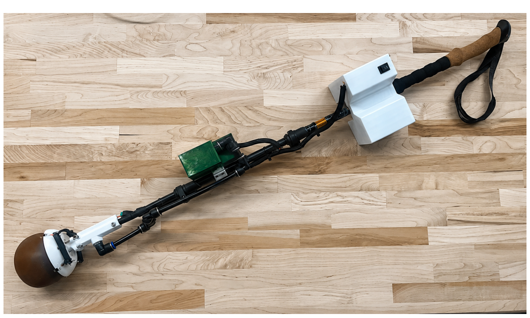

Fig. 1. Final Prototype

Fig. 2. Membrane in Soft Flexible State vs. Stiffened State

II. Methods

A. Holding Force

In the context of trekking poles, the holding force is the maximum load the structure can resist before deforming or slipping, i.e., the maximum load it can bear while maintaining its rigid, jammed state. Industry certification standards require trekking poles to withstand a minimum axial holding force of 1,400 N [3]. To meet these quality standards, a trekking pole was selected as the base platform and subsequently modified to incorporate the granular jamming mechanism.

B. Power Draw and Battery Sizing

To size the battery running our electronics we started with volumetric estimates in order to get a reference time scale of how long the pump needs to be on in order for the end-effector to reach a rigid state. With a time estimate, we then used manufacturer reported current draws to finally get an estimate total run time in hours for different battery capacities.

1) Volumetric Estimates: In an ideal world, we assume the entire pneumatic system including connectors, pipping, the end-effector, and the pump are perfectly air-tight such that we can estimate the volume of air in the system to be solely dependent on the geometric properties of each component.

For the volume of air in the pipping we took a generous estimate of roughly 0.5 m of 3/8" diameter tubing, this tubing was more than the length of our pole. To caculate the total volume of air in the tubing we used the equation for volume of a cylinder, $V = \pi r^2 l$.

Similarly, to estimate the volume of the coupler core (Fig. 3), we used the volume equation of a cylinder and the fact that by design the air-channel through the center and port for a connector share the same 3/8" diameter as the piping. The length component of the equation we got from the solidworks model with 6.27 cm^3 for the air-channel and 1.19 cm^3 for the port respectively.

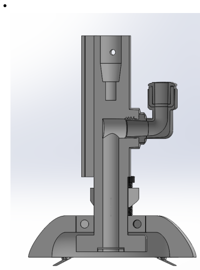

Fig. 3. Coupler Core

In the end, a majority of the volume of air was from the membrane in the end-effector. The stress ball rubber membrane we chose had an unstreched diameter of 4in, which we turned into volume with the equation for the volume of a sphere, $V = \frac{4}{3}\pi r^3$. In most literature we found surrounding granular jamming in soft-robotics, common fill percentages for small grains were around 50-60% of the membrane volume. Since these texts focused on grabbing applications which did not match the use-case of a hiking pole, we used a 95% fill percentage. This is mostly born out of our very early prototyping, where we learned that in order to maximize rigidity and stability, we needed to fill as much of the membrane with granules as possible.

Finally, we could get an estimate of the total volume of air in the system by combining the volumes of tubing, the coupler, and pump internals, then subtracting the volume occupied by coffee grounds. To turn this into a time, we averaged over three common pump volumetric flows available on Amazon, 10 L/min, 9 L/min, 8 L/min, multiplied them by our estimated air volume, and converted to cm^3/s to get a time-to-vacuum. We could not find research relating vacuum pressure in the membrane to the level of rigidness given a particular grain, so in order to make our time estimate more accurate we multiplied it by 50% to get a Modified time-to-vacuum, t_v. Based on early prototyping, we knew we could reach a rigid state even with a weaker pump and poor air seals, so we were confident that reaching a rigid state requires removing even less than 50% of the air in the system.

2) Current Draw Estimates: Our electronics were made up of an Arduino Uno, an H-bridge, and a vacuum pump. The Arduino controls the H-bridge, which manages power to the pump and feeds 5V to the Arduino. For early power estimates, we used the max current draw for both the Arduino, I_a, (50mA [4]), and the H-bridge, I_h, (36mA [5]). The pump we chose was an 81kPa pump rated for 12V and 10W of power draw ([6]), giving a peak current draw of 833.3 mA, I_p. We briefly debated including a solenoid valve in case our final prototype was air-tight enough that we could afford to only run the pump briefly, seal the end-effector, then use the solenoid to switch to an open-air connection to quickly refill the membrane with air. The three way solenoid valve we considered drew 6.5W of power and ran on 12V ([7]), giving a current draw, I_s, of 640 mA.

To best inform our battery capacity we came up with three scenarios of battery use, running the pump continuously, running the pump for half the gait cycle of a theoretical user, and running the pump until rigid then sealing the end-effector with a solenoid valve. For all scenarios, given a particular battery capacity, B_C in milli-Amp hours, the total use time, t, in hours is $t = B_c/I$, where I, is the total current draw.

The first scenario is the simplest, assuming a worst case where the pump is always at max power. Where total current draw is, $I = I_a + I_h + I_p$.

In the second scenario, we run the pump as long as the pole is pressed against the ground, and if the user only presses the pole against the ground for half of their stride duration (one legs worth of motion), then the pump is only on half the time. Generalizing, we came up with an Effective Pump Current Draw Coefficient, C_P, of 0.5 which just means the pump is running half of the time. This makes the total current draw, $I = I_a + I_h + C_p I_p$.

For the third scenario we take the membrane to rigidity using the modified time-to-vacuum from the volumetric calculations, and seal the membrane with a solenoid valve until the pole is lifted off the ground. Since this depends on how long the pole is pressed against the ground we started with gait data [8] for four groups, Male, Female, people 18-25 years old, and 30-38 years old. In particular, we got stride time data, t_s, or the average time each group takes to complete a full walking cycle. To get an Effective Pump Current Draw Coefficient, C_p, we calculate the percent time the pump is on during a walking cycle, $C_p = \frac{t_v}{t_s}$. Then, if the pole is only on the ground for the remainder of a single step (half of the walking cycle), we can calculate how long the solenoid needs to be on with $t_{sol} = t_v - \frac{t_s}{2}$. Finally, we can get an Effective Solenoid Current Draw Coefficient, C_s with, $C_s = \frac{t_{sol}}{t_s}$, or how much of the time the solenoid is running. This gives a total current of $I = I_a + I_h + C_p I_p + C_s I_s$.

C. Coupler Material and Structure

The coupler is the structural component that connects our granular jamming end-effector to the trekking pole therefore we wanted to run a FEA on it to validate structural strength. The geometry and structure of the coupler were designed to accommodate 3/8 NPT fittings & piping and 6-32 bolt & heat set inserts fasteners [9] [10]. This influenced design choices such as edge thickness. Our current prototype uses a coupler that is made of 3D-printed PLA with custom print settings of four solid walls, 70% infill, and gyroid infill pattern. We found through trial and error that four solid walls provided enough solid material for tapping of 3/8 NPT threads [9]. 70% infill and gyroid infill pattern were chosen for structural strength purposes. Since we used a custom printed PLA we had to find its material properties before we can run a FEA on this part.

1) Custom Material Properties: To run a FEA we needed to find the ultimate tensile strength, yield strength, Young's modulus, Poisson's ratio, and density. Density can be simply calculated by weighing the coupler with a scale for the mass and getting the volume from the CAD.

$$\rho = \frac{m}{V} \tag{1}$$

To get the other material properties, a tensile test was ran on a dogbone specimen printed out of this custom PLA using an Instron 5569A (Fig. 4). This gave us a data set of axial force, axial strain, and lateral strain, which allowed for stress-strain analysis.

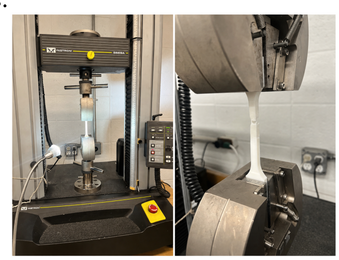

Fig. 4. Tensile Testing of PLA Dogbone

Simplifying Hooke's law in the axial direction (Appendix) results in the relationship for the Young's modulus:

$$\epsilon_{yy} = \frac{1}{E}(\sigma_{yy} - \nu\sigma_{xx}) \tag{2}$$

$$E = \frac{\sigma_{yy}}{\epsilon_{yy}} \tag{3}$$

Young's modulus can be experimentally determined using the collected tensile testing data. Specifically, a linear fit can be applied to the stress-strain data (σ_{yy} vs. ϵ_{yy}) within the linear elastic region. The slope of this is the material's Young's modulus.

Using the same stress-strain data, the yield strength (σ_y) is found by using the 0.2% offset method where line parallel to the linear elastic slope is shifted by a strain of 0.002. The intersection of this offset line with the experimental stress–strain curve defines the yield strength. More easily, the ultimate tensile strength (σ_u) is determined by taking the maximum stress value of the stress-strain curve.

Lastly, to calculate the Poisson's ratio, Hooke's law in the lateral direction is simplified (Appendix):

$$\epsilon_{xx} = \frac{1}{E}(\sigma_{xx} - \nu\sigma_{yy}) \tag{4}$$

$$\nu = -\frac{\epsilon_{xx}}{\epsilon_{yy}} \tag{5}$$

To obtain the Poisson's ratio from experimentally, lateral strain can be plotted against axial strain (ϵ_{xx} vs. ϵ_{yy}). A linear fit can be performed on the data points in the linear elastic region of the material. The negative of the slope of this best-fit line provides the experimental value for Poisson's ratio.

2) FEA Methodology: Once the material properties were calculated, to begin the FEA, the coupler was further simplified into this T-shape cylinder (Fig. 5) since the lip portion is the main geometry we're concerned with taking loads.

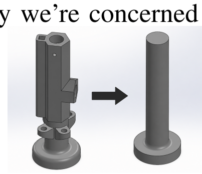

Fig. 5. Simplification of Coupler

Then fixtures and a load are applied to this simplified model of the coupler (Fig. 6). The main body top of the coupler was assumed to be fixed since it is fully engaged with the pole. The coupler geometry was loaded at the base with 30% of the average male weight of 90.6 kg which equates to approximately 266.6 N since hikers transfer at most 30% of their body weight through their arm during pole use [1]. Assuming the worst case, all the load would be acting on the bottom face at a 45° so that it is applied axially and laterally.

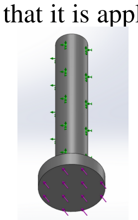

Fig. 6. Fixture and Loading of Coupler

With the fixture and loading applied, mesh analysis was ran (Fig. 7). Three meshes with 12 elements in 360° of progressively finer meshes going from element sizes of 3.6 mm to 2.7 mm to 1.8 mm were used. Since PLA is a brittle material the analysis is based on the max principal normal stress and a Factor of Safety threshold of 6 was chosen. A mesh convergence is confirmed by validating if percent changes in max principal normal stress over the number of elements between meshes are less than 5%. Lastly, the max principal normal stress and Factor of Safety plots are observed for the finest mesh. The FEA results was then validated with an experimental setup described in the next section.

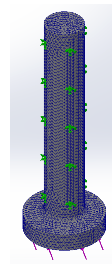

Fig. 7. Finest Mesh Model

D. Shear Load Physical Testing

Shear loading of the coupler was evaluated by clamping the coupler horizontally and suspending a bucket of known weights directly from it. The coupler was loaded incrementally up to 50 lb. The setup for this test is shown in Fig. 8.

Fig. 8. Shear loading test setup.

E. Puncture Tests

Puncture resistance of the membrane was evaluated by pressing and dropping (Fig. 9 and Fig. 10) the membrane directly onto sharp implements, including scissors and box cutters. For the press-puncture test, a compressive load of approximately 54 lb (240 N) was applied manually, representing an estimated 30% of the body weight of a 180 lb user transferred through the arm during pole use [1], yielding an applied force of $180 \times 0.30 = 54$ lb (≈ 240 N). It should be noted that the 180 lb figure was obtained by averaging out the average female body weight of 170 lb and the average male body weight of 198 lb [11]. Additionally, all puncture tests were performed by a team member weighing 180 lb.

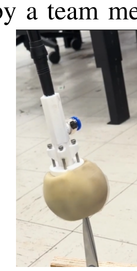

Fig. 9. Press puncture test of membrane.

The membrane drop test was conducted by releasing the membrane from a height of approximately 6 inches, simulating the impact load experienced if the pole were dropped by a standing user onto a sharp object during typical use.

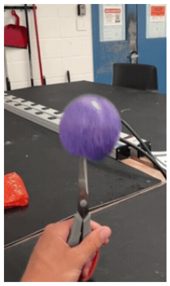

Fig. 10. Membrane being dropped onto scissors.

III. Results

A. Qualitative Observations

Results for design constraints, including membrane puncture results and the coupler shear strength, were evaluated through a series of pass/fail tests and can be referenced in Table I.

TABLE I

Membrane and coupler mechanical test results.

Test	**Condition**	**Result**
Puncture – sharp objects	Scissors, box cutters	Pass
Puncture – compressive load	54 lb (240 N)	Pass
Puncture – drop test	6 in drop	Pass
Shear – coupler	50 lb (222 N) suspended load	Pass

From Fig. 11 it can be seen that the subsequent membrane and coupler used in both the puncture and shear test had no visual indicators of a failed qualitative test. The membrane held intact after the puncture tests, and the coupler showed no visible signs of deformation from the shear loading.

Fig. 11. Aftermath of shear loading and puncture tests.

B. Electrical Characteristics

With the assumptions outlined in the Methods, we got the following Volume of Air estimates for each component of the pneumatic system.

TABLE II

Volume Estimates

Part	Volume Estimate (cm^3)
Nylon 3/8" Piping	0.3
Membrane	4393.1
Coupler	5.3
Pump	4
Coffee Grounds	4173.4
Total	229.3

Using common volumetric flows for generally available small vacuum pumps we got an average Modified time-to-vacuum of $t_v = 0.77s$ based on the volume estimates in Table II.

TABLE III

Modified time-to-vacuum

Vol. Flow (L/min)	Vol. Flow (cm^3/s)	t_v (s)
10	166.67	0.69
9	150	0.764
8	133.3	0.86

Using data from the National Library of Medicine [8], we calculated running times per gait cycle for the pump and the solenoid using the equations outlined in the methods for the third battery use scenario.

TABLE IV

Pump/Solenoid-On Time per Gait Cycle

Group	Stride Time	Pump-On Time	Solenoid-On Time
Male	1.145	0.771	0.198
Female	1.135	0.771	0.203
18-25	1.135	0.771	0.203
30-38	1.14	0.771	0.201
Avg.	1.139	0.771	0.201

Using averaged values this gave us Effective Pump/Solenoid Current Draw Coefficients of C_p=0.67 and C_s=0.18. Now, we could get effective total current draws and expected battery life for all three battery scenarios across common battery capacities.

TABLE V

Effective Total Current Draw & Battery Life

Eff. Current (mA)	Always On	50% On	Pump & Solenoid
	919.33	502.67	763.26
Battery Life (hours)			
6000 (mA-h)	6.53	11.94	7.86
5000 (mA-h)	5.44	9.95	6.55
3000 (mA-h)	3.26	5.97	3.93
2000 (mA-h)	2.17	3.98	2.62

Finally, using a power supply to drive just the pump while attached to the rest of the pneumatic system including piping and the coupler, it only used about 0.4-0.5 Amps of current. Even when connecting the pump to the H-bridge, and the H-bridge to the Arduino current use never went above 0.5 Amps.

C. Custom PLA Material Properties

After graphical analysis (Appendix) on the tensile testing data using Eq. 3 and Eq. 5, ultimate tensile strength, yield strength, Young's modulus, and Poisson's ratio were found. Density was also calculated using Eq. 1. The material properties for this 3D-printed PLA with custom print settings is acquired and shown in Table VI.

TABLE VI

Custom PLA Material Properties For FEA

σ_u **(MPa)**	σ_y **(MPa)**	E **(MPa)**	ν	ρ **(kg/m^3)**
27.38	24.403	2782.6	0.309	929.95

D. Coupler FEA Results

Following mesh analysis of three increasingly finer meshes, the number of elements of each mesh and their respective max principal normal stress shown in Table VII is evaluated in a mesh convergence plot for percent change in Fig. 12. With this the finest mesh model plots (Fig. 13) for the max principal normal stress and Factor of Safety can be observed where the maximum failure stress is 3.403 MPa and the highest stress areas of green have a Factor Safety around 6-7.

TABLE VII

MESH ELEMENTS AND RESPECTIVE STRESS

Number of Elements	Max Principal Normal Stress (MPa)
12900	3.507
26314	3.436
63729	3.403

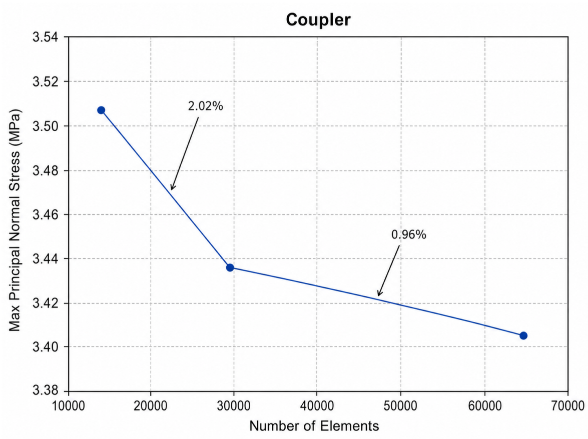

Fig. 12. Mesh Convergence Plot With Percent Change

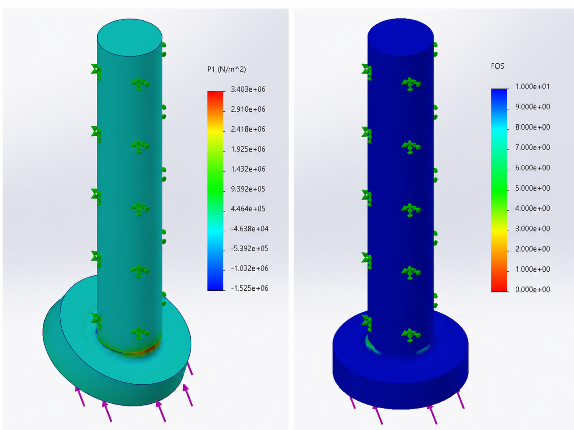

Fig. 13. Finest Mesh Plots

IV. DISCUSSION & CONCLUSION

A. Puncture Tests

The membrane successfully passed all qualitative puncture evaluations; however, the testing methodology was limited in rigor. Puncture resistance was assessed by manually pressing sharp implements against the membrane surface and observing whether failure occurred, rather than through instrumented force measurement. Several assumptions introduced uncertainty into the mechanical testing. The compressive load of 54 lb was estimated based on an assumed 30% body weight transfer through the arm [1], rather than measured directly. Similarly, the drop height of 6 in and the use of sharp implements such as scissors and box cutters were selected based on the judgment of the sharpest objects available, rather than on a standardized test protocol. Future work should adopt a more controlled methodology, such as using a materials testing machine to apply precise, repeatable loads and quantitatively measure the force at failure rather than relying on a binary pass/fail system.

B. Shear Load Physical Testing

TÜV SÜD certification standards require trekking poles to withstand a minimum axial load of 1,400 N (315 lb) [3]. The shear test conducted in this work loaded the coupler to only 50 lb (222 N), well below this benchmark. Although the coupler exhibited no failure under the tested load, it cannot be concluded that the design meets industry certification standards without further testing to failure at higher loads. From the perspective of the physical testing, the actual safety factor is unknown due to the test being stopped after 50 lb. To fully characterize the shear strength, future testing should load the coupler incrementally until failure to establish a definitive breaking point. Future work should also test multiple printed couplers to account for vulnerabilities in the 3D-printed material. Additionally, the bucket loading method, while practical, introduces minor dynamic loading due to the swinging of the bucket as weights are added, which deviates from a purely static shear condition. A more controlled approach would use a materials testing machine to apply a precise, quasi-static shear load directly to the coupler.

C. Electrical System

Based on the Battery Life results from V, we decided on a 6000 mA-h battery. Hike times can vary widely from user-to-user so for the purposes of prototyping we chose a battery that lasted the length of an all day hike. We expect the pump to be on between 50-100% of the time, which gives between 6-12 hours of use on full charge. This extra leeway also helps account for battery decay due to continuous charge cycles. The pump motor accepts input voltage of 9-12V which allows the motor to stay running for up to 90% of the life of the battery. This was determined through draining the battery and determining when the output voltage passed the 8.9V threshold. Originally, we expected our current draw to be slightly higher than our estimates since due to heat loss from the H-bridge. However, in practice we found that the pump's max current draw when attached to the prototype rarely went over 0.5 Amps which is lower than the 0.83 Amps in our estimates. So even though the power draw of the H-Bridge might be above our estimate, the lower power draw of the pump more than makes up for the H-bridge.

As for the Solenoid-Pump combination, the extra battery life from reducing the work done by the pump by including the solenoid was not enough to justify the extra weight and complexity. Therefore, we focused solely on the pump and implemented sensing to ensure that it is on only when needed. In the final prototype, we did this with limit switches wired in parallel at the base of the pole. When a limit switch closes due to the membrane making contact with a surface, the Arduino actuates the pump, closing the loop.

D. Coupler FEA and Structure

The mesh convergence analysis shown in Fig. 12 confirmed that the FEA showed valid mesh convergence as percent changes of 2% and less than 1% both fall within the threshold of 5%. This meant that there was valid mesh refinement for the FEA. Since there was valid mesh refinement, the FEA values can be taken as a good estimate. Taking the maximum principal normal stress of 3.403 MPa in relation to the ultimate tensile strength of 27.38 MPa results in a Factor of Safety of 8 and the highest stress areas highlighted green in Fig. 13 have a Factor of Safety of around 6-7. From the FEA, it can be seen that this 3D-printed PLA with custom print settings will hold for our use case, as based on the criteria for brittle material failure, a Factor of Safety of at least 6 was achieved. The FEA is also validated with the experimental setup in Fig. 8 where we used 50 lbs which is about the same load as the FEA but at an even more extreme case of shear. Since the shear loading held this further proves that our FEA is a good estimate and our coupler made of this custom printed PLA will hold for its intended use case. However, for a future design we would manufacture the coupler out of aluminum to make sure it is well above the Factor of Safety threshold and for a refined, commercial look.

Even though our FEA was supported by an experimental setup and proved to be a reasonable estimate, there were still limitations in the analysis that may have introduced error and prevented the simulation from being even more accurate. The main limitation was the material assumption. Because the part was 3D-printed using PLA, the material contained layer lines and directional differences in strength relative to the print orientation, meaning it behaves anisotropically rather than isotropically. For our tensile testing and FEA, we didn't account for this as this anisotropic behavior would have made the analysis significantly more complex than necessary for an estimation-based study. We also assumed that the use of additional solid walls, higher infill density, and a gyroid infill pattern would reduce the effects of anisotropy enough to make the model reasonable for approximation purposes [12]. In the future, the accuracy of the analysis could be improved by using a more advanced simulation tool, such as ANSYS, instead of relying only on SolidWorks. A more detailed model could include anisotropic material properties, print direction dependent strength, and more accurate representation of the internal infill structure. Additional tensile tests using specimens printed in different orientations could also be used to define material properties more accurately. These improvements would allow the simulation to better capture the real behavior of 3D-printed PLA.

E. Conclusion

This work presented the design, fabrication, and preliminary mechanical evaluation of a granular jamming trekking pole aimed at improving stability and accessibility for hikers with limited mobility. The core mechanism - a vacuum-driven granular jamming system using coffee grounds encased in a flexible membrane - was successfully integrated into a prototype that showed off its benefits and uses.

Qualitative mechanical testing methods demonstrated that the membrane withstood puncture from sharp implements, a compressive load of 54 lb, and a 6 in drop without failure. The 3D printed coupler similarly showed no signs of deformation under a shear load of 50 lb. While these results are encouraging, the testing methodology was limited in rigor, relying heavily on manual observation.

The electrical system exceeded expectations: the pump drew considerably less current in practice than estimated, resulting in a projected battery life well-suited for full-day hiking. A key design decision was to eliminate the solenoid-pump combination in favor of a pump-only system, as the marginal gains in battery life from the solenoid did not justify the added weight and complexity. Instead, sensing was implemented using limit switches wired in parallel with the Arduino's internal pull-up resistor, ensuring that the pump activates only when the pole contacts ground. This approach successfully balanced simplicity and power efficiency in the final prototype.

Future work should focus on three key areas: instrumented mechanical testing to quantitatively characterize the membrane puncture threshold and the coupler failure load, optimization of the 3D-printed coupler geometry and print orientation to improve shear strength, and user testing to evaluate real-world performance and actuation response time under field conditions. With these improvements, the granular jamming trekking pole represents a promising platform for further development into a viable assistive hiking device.

V. Appendix

A. Material Properties Derivation

Under ideal uniaxial tensile loading, a single externally applied force F acts along the loading axis (defined here as the y-direction). No externally applied tractions act on the transverse faces, and therefore the lateral normal stress and in-plane shear stress vanish. The resulting stress state is:

$$\sigma_{yy} = \frac{F_{yy}}{A_0} = \frac{F_{yy}}{w_0 t_0} \tag{6}$$

$$\sigma_{xx} = 0 = \sigma_{xy} \tag{7}$$

where $A_0 = w_0 t_0$ is the original cross-sectional area of the dogbone specimen's gage section.

Then by applying Hooke's law in two dimensions, the relationship between axial strain and the stress components can be derived:

$$\epsilon_{yy} = \frac{1}{E}(\sigma_{yy} - \nu\sigma_{xx}) \tag{8}$$

As previously established in Eq. 7, the lateral stress is zero for this uniaxial test. Therefore, Hooke's law reduces to a relationship between axial stress and strain:

$$\epsilon_{yy} = \frac{\sigma_{yy}}{E} \tag{9}$$

This can be rewritten to express Young's modulus as the ratio of axial stress to axial strain:

$$E = \frac{\sigma_{yy}}{\epsilon_{yy}} \tag{10}$$

Next using Hooke's law for the lateral direction:

$$\epsilon_{xx} = \frac{1}{E}(\sigma_{xx} - \nu\sigma_{yy}) \tag{11}$$

Combining this with Eq. 7 and Eq. 10. We get a relationship between lateral strain to the axial stress:

$$\epsilon_{xx} = -\nu\epsilon_{yy} \tag{12}$$

Poisson's ratio can then be displayed as the following:

$$\nu = -\frac{\epsilon_{xx}}{\epsilon_{yy}} \tag{13}$$

B. PLA Material Properties Analysis

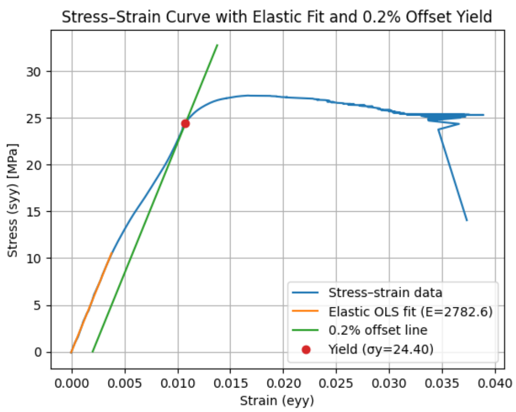

Fig. 14. Graphical analysis of axial stress vs. axial strain

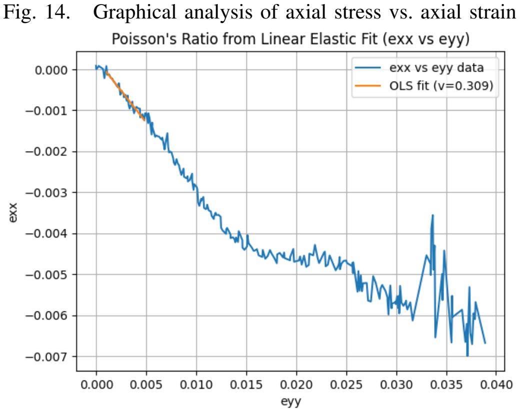

Fig. 15. Graphical analysis of lateral strain vs. axial strain

References

[1] A. Hawke and R. Jensen, "Are trekking poles helping or hindering your hiking experience? a review," *Wilderness Medical Society*, vol. 31, no. 4, 2020.

[2] S. Hauser, M. Robertson, A. Ijspeert, and J. Paik, "Jammjoint: A variable stiffness device based on granular jamming for wearable joint support," *IEEE Robotics and Automation Letters*, vol. 2, no. 2, pp. 849–855, 2017.

[3] TÜV SÜD Product Service GmbH, "Certification mark for trekking poles." https://www.tuvsud.com/en/customer-hub/ps-cert/certification-mark-for-trekking-poles, 2024.

[4] Arduino, "Arduinostore." https://store-usa.arduino.cc/products/arduino-uno-rev3.

[5] H. Technology, "L298n dual h-bridge motor driver." https://www.handsontec.com/dataspecs/L298N

[6] VN-T1, "Vacuum pump, vn t1 10 l min dc small vacuum pump, 81 kpa negative pressure (dc 12v)." https://a.co/d/0156QrNE.

[7] MECCANIXITY, "Meccanixity 3/8 inch pneumatic valve 12v, 3 way 2 position electric air solenoid valve manual control outlet wire." https://a.co/d/0421GsHF.

[8] T. Abualait and M. Ashan, "Comparison of gender, age, and body mass index for spatiotemporal parameters of bilitateral gait pattern," *National Library of Medicine*, 2022.

[9] M. Doctor, "National pipe thread: Charts and formulas (npt)," n.d.

[10] U. M. D. Lab, "Heat set inserts," n.d.

[11] Centers for Disease Control and Prevention, "Body measurements." https://www.cdc.gov/nchs/fastats/body-measurements.htm, 2025. Accessed: May 2026.

[12] Markforged, "3d printing settings impacting part strength," n.d.